Pickeringite from the Stone Town Nature Reserve in Ciężkowice (the Outer Carpathians, Poland)

Mariola Marszałek * , **Adam Gaweł and Adam Włodek**

Department of Mineralogy, Petrography and Geochemistry, AGH University of Science and Technology, al. Mickiewicza 30, 30-059 Kraków, Poland; agawel@agh.edu.pl (A.G.); wlodek@agh.edu.pl (A.W.)
* Correspondence: mmarszal@agh.edu.pl

Abstract: Pickeringite, ideally $MgAl_2(SO_4)_4 \cdot 22H_2O$, is a member of the halotrichite group minerals $XAl_2(SO_4)_4 \cdot 22H_2O$ that form extensive solid solutions along the joints of the X = Fe-Mg-Mn-Zn. The few comprehensive reports on natural halotrichites indicate their genesis to be mainly the low-pH oxidation of pyrite or other sulfides in the Al-rich environments of weathering rock-forming aluminosilicates. Pickeringite discussed here occurs within the efflorescences on sandstones from the Stone Town Nature Reserve in Ciężkowice (the Polish Outer Carpathians), being most probably the first find on such rocks in Poland. This paper presents mineralogical and geochemical characteristics of the pickeringite (based on SEM-EDS, XRPD, EPMA and RS methods) and suggests its possible origin. It belongs to the pickeringite–apjohnite (Mg-Mn joints) series and has the calculated formula $Mg_{0.75}Mn_{0.21}Zn_{0.02}Cu_{0.01}Al_{2.02}(S_{0.99 \text{ to } 1.00}O_4)_4 \cdot 22H_2O$ (based on 16O and $22H_2O$). The unit cell parameters refined for the monoclinic system space group $P2_1/c$ are: $a = 6.1981(28)$ Å, $b = 24.2963(117)$ Å, $c = 21.2517(184)$ Å and $\beta = 100.304(65)°$. The Raman spectra (SO_4) bands are the intensive 994 cm^{-1} and a low-intensive 975 cm^{-1} (ν_1), low-intensive 1081, 1123 and 1145 cm^{-1} (ν_3), 524, 467 and 425cm^{-1} (ν_2), 615 cm^{-1} (ν_4), while those at 344 and 310 cm^{-1} are attributed to ν_g H_2O and at 223 cm^{-1} to the lattice modes. Crystallization of pickeringite within the particular tor resulted from a certain set of conditions: climatic (e.g., season, temperature, humidity), physicochemical (e.g., pH, concentration), mineral (the presence of pyrite), and site-related (location and efflorescence protection). The sulfate ions could have been derived from oxidation of pyrite in the Ciężkowice sandstones and possibly are related to local mineral waters.

Keywords: pickeringite; halotrichites; efflorescence; sandstone; Ciężkowice; the Carpathians; Poland

1. Introduction

Pickeringite is a hydrated double sulfate that belongs to the halotrichite mineral group. The general formula of halotrichite is $XY_2(SO_4)_4 \cdot 22H_2O$, i.e., $XSO_4 \cdot Y_2(SO_4)_3 \cdot 22H_2O$, where X is mainly Co^{2+}, Fe^{2+}, Mg^{2+}, Mn^{2+}, Ni^{2+} and Zn^{2+}, while Y is Al^{3+}, Cr^{3+} and Fe^{3+}. The minerals of the group are referred to as pseudo-alums due to their relation to the alum group minerals $RY(SO_4)_2 \cdot 12H_2O$, i.e., $R_2SO_4 \cdot Y_2(SO_4)_3 \cdot 24H_2O$, where R represents an univalent cation such as ammonium, sodium, potassium, or cesium [1–3]. When a divalent cation, such as manganese, ferrous iron, cobalt, zinc or magnesium, is introduced instead of the univalent cation the, minerals form the halotrichite series that is not isomorphous with the monovalent alums. The halotrichites crystallize in the monoclinic space group $P2_1/c$ and are all isomorphous within their family [4,5]. In contrast to mixed crystals, halotrichites of the ideal composition, i.e., corresponding to the theoretical end-member formulae, are rare in the nature. Isomorphic substitutions result in complete solid solutions that can exist among the various end members of this mineral series.

According to the published data, mixed crystals between pickeringite $MgSO_4 \cdot Al_2(SO_4)_3 \cdot 22H_2O$, the Mg^{2+} end-member of the group of halotrichites, and its Fe^{2+} analogue halotrichite $FeSO_4 \cdot Al_2(SO_4)_3 \cdot 22H_2O$ can exist, and such miscibility extends also towards the Mn^{2+} end-member apjohnite $MnSO_4 \cdot Al_2(SO_4)_3 \cdot 22H_2O$ and other known end members of the group (e.g., Zn^{2+} dietrichite and Co^{2+} one wupatkiite) [1,4–8].

The halotrichites originate mainly from oxidation of pyrite or other sulfides in ore deposits in aluminum-rich environments due to, for instance, weathering of rock-forming aluminosilicates under low pH conditions [2,9,10]. However, the halotrichites require both favorable local ionic activities and specific atmospheric conditions. Being highly soluble salts [6], they crystallize within open rock spaces in arid climates but in normal humid climates they cannot occur during the wetter part of the year if the rock spaces are exposed to precipitation. Under such conditions, the halotrichites can be formed in rain-protected locations such as rock niches or under overhangs.

Halotrichites may be constituents of rock efflorescences, where they are frequently found in association with other sulfates, such as alunogen $Al_2(SO_4)_3 \cdot 17H_2O$, hydrated Mg sulfates (e.g., epsomite $MgSO_4 \cdot 7H_2O$ and hexahydrite $MgSO_4 \cdot 6H_2O$), melanterite $FeSO_4 \cdot 7H_2O$, copiapite $(Fe^{2+},Mg)Fe^{3+}_4(SO_4)_6(OH)_2 \cdot 20H_2O$, K-alum $KAl(SO_4)_2 \cdot 12H_2O$, and gypsum $CaSO_4 \cdot 2H_2O$ [11–17]. They are often found in sulfide-bearing ore mines, especially the abandoned ones, in waste dumps of such deposits [10,11,13], tailing dumps [18], coal mines and self-burning dumps of coal mining waste (e.g., [19–22]), weathered pyrite-bearing rocks such as schists, shales, lignites, gneisses (e.g., [9,12,23,24]), occasionally sandstones [25], sulfuric acid caves [26], and also in the sandstones and gneisses used as stone building materials in historical places [27,28].

Pickeringite and other halotrichite group minerals are known from a few locations in Poland, including the abandoned workings of the Staszic iron sulfide ore mine at Rudki near Nowa Słupia; the Holy Cross Mts [29,30]; menilite shales of the Carpathians [17,31]; the Poznań clays series at Dobrzyń on the Vistula River [32,33]; pyrite-bearing sericite-chlorite schists in Wieściszowice, Lower Silesia; mica schists in a quarry at Krobica, the Sudety Mts, Lower Silesia [15,16,34]; self-burning coal-mining waste dumps in the Upper and Lower Silesian Coal Basins [8,35]; and the Shale Formation in the Pieprzowe Mts [17,36,37].

The pickeringite in question was found in the efflorescences on the sandstone tors from the Stone Town Nature Reserve (further referred to as STNR) in Ciężkowice in the Outer Carpathians, Poland [38]. The paper presents comprehensive microscopic (SEM-EDS), X-ray powder diffraction (XRPD), electron microprobe analysis (EPMA), and Raman microspectroscopy (RS) data to identify detailed mineralogical and geochemical characteristics of the mineral and to discuss its possible genesis. According to our knowledge, it is the first detailed report on the pickeringite occurring on sandstones in Poland.

2. Geological Setting

The Stone Town Nature Reserve is located in the Ciężkowice village (49°46′36″ N, 20°57′50″ E) within the Ciężkowice Foothills (the Silesian Nappe) of the Outer Flysch Carpathians, in the eastern part of the Ciężkowice-Rożnów Landscape Park (182.47 km²) established in 1995. The STNR was already protected in 1930 and revived after the Second World War in 1974, and now it covers a surface of 0.15 km² [39]. A remarkable geographical signature of the STNR is picturesque sandstone landforms, occupying a small area as a group of relatively large, separated from each other tors with the shapes of towers and pulpit-like rocks, scattered in a pine forest [40–42]. Within the reserve, there are 11 groups composed of such rocky forms ranging in height from 5 to 17 m, accompanied by many smaller forms of 3–5 m in height [43] (Figure 1). They are distributed mainly on a hill slope of the relative altitude of 100 m, that spans the area from the flood terrace of the Biała River to the extensive hill culmination (a plateau at 360 m a.s.l.).
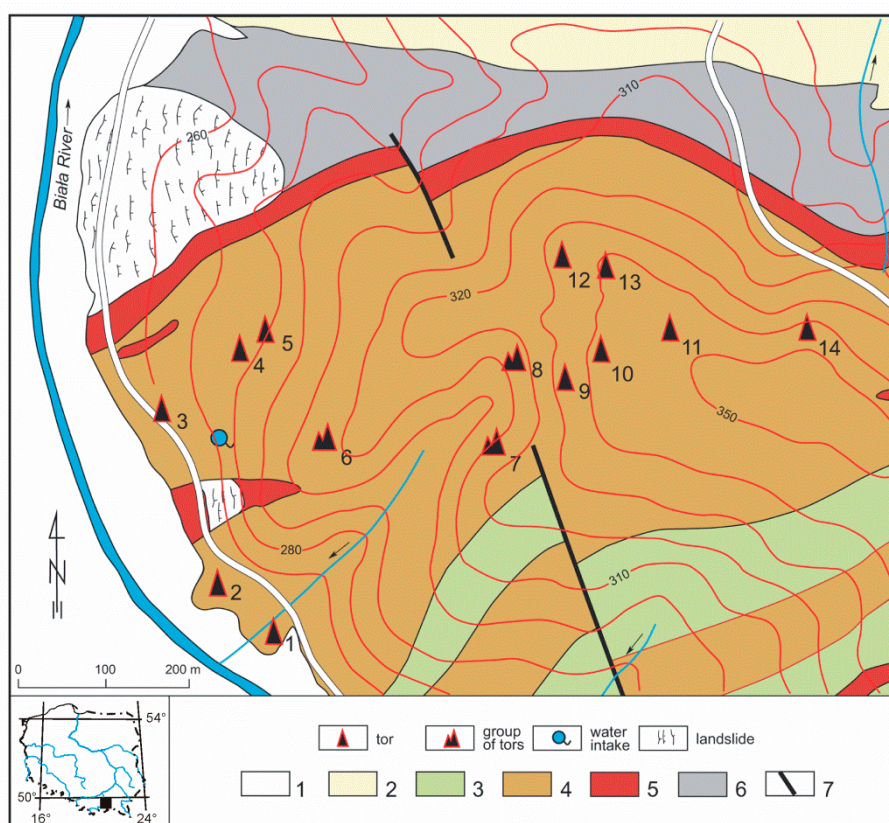
Figure 1. Distribution of the sandstone tors on the geological map of the Stone Town Nature Reserve (STNR), Ciężkowice area (after [43–45], modified). Quaternary deposits: 1, alluvial clays; 2, alluvial and deluvial loams. Paleogene flysch sequences: 3, Hieroglyphic Beds (green shales and sandstones); 4, Ciężkowice Sandstones (conglomeratic sandstones, sandstones, conglomerates); 5, Variegated and Red Shales (shales); 6, Upper Istebna Shales (shales); 7, fault.

The area of the stone town in Ciężkowice is a stratotype locality of the Upper Paleocene to Lower Eocene Ciężkowice Sandstone Formation. The thickness of this horizon reaches 350 m and the sandstone represents classical fluxoturbidites, called at present the debris flows or fan deposits [44–47]. The thick-bedded sand-and-gravel strata are exposed as single rocky forms or their groups, being more resistant to weathering than shale-and-sandstone strata of the Carpathian flysch. The Ciężkowice Sandstone occurring within the STNR form three thick lenses developed as thick-bedded (mainly 1–4 m) conglomeratic sandstones, sandstones, and conglomerates. The rocks, mainly conglomerates, contain clasts represented prevalently by claystones and, occasionally, limestones that range from one to several centimeters in size. The protected rocky landforms occur mainly as the outcrops of the stratigraphically lowermost (III) horizon of the Ciężkowice Sandstone, Early Eocene in age [43,48]. The dominating lithofacies of the IIIrd horizon are represented by the conglomeratic sandstones containing dispersed pebbles. The Sandstone Formation, cropping out in the nature reserve, is underlain by the Lower to Middle Eocene Variegated Shales and overlain by the thin-bedded shale-and-sandstone Hieroglyphic Beds of the Middle Eocene or younger shale series [43]. The shapes of the Carpathian sandstone tors mainly depend on the arrangement of joint fractures that have disintegrated the rock massif following the directions of decompressional and gravitational movements. These processes took place in the Quaternary, particularly at the very end of the Pleistocene and in the Holocene. The process of rock surface carving was continued due to selective weathering and was stimulated by the character of denudation. Differences in resistance of individual sandstones beds and their depositional differentiation are demonstrated by the rich microrelief and exposition of the hardest rocks [39,43].

### 3. The Ciężkowice Sandstones and their Efflorescences

The Ciężkowice sandstones are classified mainly as quartz arenites and wackes, occasionally subarcose or feldspathic wackes [45,49,50]. They are composed of quartz, feldspars (orthoclase, occasionally microcline and plagioclases, often altered to sericite and/or kaolinite), rock fragments, and micas (biotite and muscovite). Rutile, anatase, zircon, tourmaline, and opaque minerals (among them pyrite) appear as accessory phases. The cement formed by matrix and occasional carbonates is of a mixed porous-contact nature. The matrix, pigmented in places by iron (oxyhydr)oxides, contains kaolinite and illite with minor interstratified illite-smectite group of minerals. Microcrystalline quartz has also been reported as one of the matrix components [51]. Granular aggregates of glauconite occur as a minor admixture. Spherical microaggregates of pyrite framboids and/or their alteration products were sometimes observed [38,52]. The average porosity of the Ciężkowice sandstones from the Stone Town tors is 6.78% [52], reaching 12.0% in the weathered varieties [38].

The weathered surface of the sandstone tors is covered in places by hard crusts composed mainly of iron minerals (among others hematite Fe_2O_3 and goethite $FeOOH$) and various salts that may also occur in the form of very thin layers as subflorescences beneath the surface [52,53]. The salts include mainly gypsum $CaSO_4 \cdot 2H_2O$ and potassium alum $KAl(SO_4)_2 \cdot 12H_2O$, occasionally accompanied by jarosite $KFe^{3+}_3(SO_4)_2(OH)_6$, barite $BaSO_4$, and halite $NaCl$ [30,52,54,55]. The efflorescences sometimes cover wider surfaces of the tors, as their crystallization and preservation depend on the atmospheric conditions and rock exposition. The salt associations differ in their composition, which depends on the dampness of the various sandstones they rest on or within. The dampness is in turn controlled by the position of the tors across the stream valley (bottom, slope, etc.) and the tor part (niche or rock face) where the precipitation took place [38]. The flake salt aggregates that occur on the tors exposed on the valley slopes, in the zones of recurring rock dampening and drying, contain mainly gypsum and syngenite $K_2Ca(SO_4)_2 \cdot H_2O$ with an admixture of K-alum. The botryoidal salt accumulations from the tors with lower parts permanently damp, i.e., those located near the valley bottom immediately over the floodplain or on lower terraces, are composed mainly of alunogen $Al_2(SO_4)_3 \cdot 17H_2O$ and pickeringite $MgSO_4 \cdot Al_2(SO_4)_3 \cdot 22H_2O$ with an admixture of gypsum [38]. The differing phase compositions of these two mineral parageneses result in the chemical differences among two types of the efflorescences. The sulfates mainly of calcium and potassium prevail in the first one, whereas the sulfates mainly of aluminum and aluminum-magnesium dominate in the second one, indicating possible local differences in the composition and pH of the parent solutions from which the salts precipitated.

The characteristic components of the variegated shales underlying the Ciężkowice sandstone are illite, chlorite, and quartz, as well as kaolinite, smectite, and vermiculite. Interstratified clay group of minerals, feldspars, carbonates and hematite are minor components [45].

4. Materials and Methods

The efflorescences containing pickeringite were collected during the summer period from the Ratusz (Town Hall) tor (no. 2 in Figure 1). The Ratusz tor is 12 m high and rises above the accumulation terrace of the Biała River (265 m a.s.l). The efflorescences occur in a niche (Figure 2). The rocks of the niche reveal joint fractures and, in the zone of weathering, additional finer fractures. Both types of fractures could form conduits for circulating waters from which secondary mineral phases could crystallize within the outer, weathering rock layers. The samples come from sheltered areas in the roof of the niche exposed to SW, at a height of 3 m from the tor bottom. The efflorescences have the form of white-beige, brittle, botryoidal accumulations of granules with a diameter of about 3 mm.
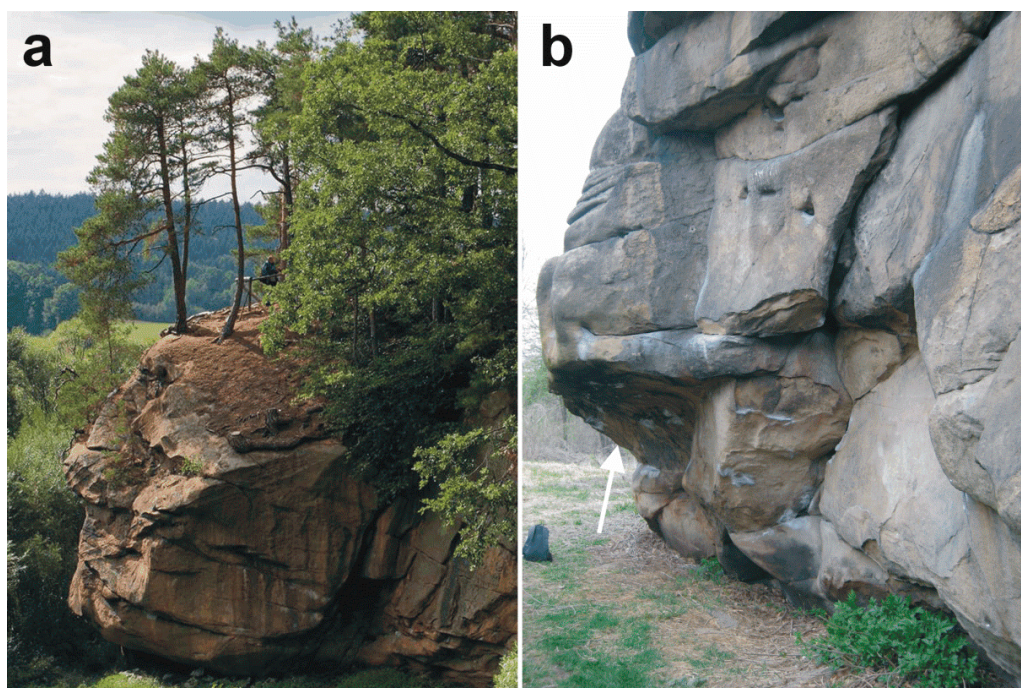
Figure 2. The Ratusz (Town Hall) tor in the STNR (**a**,**b**; for location details see Figure 1—tor 2), and the niche with white-beige pickeringite efflorescences marked in (**b**).

In addition, taking into account seasonal changes in prevailing weather conditions, we would like to check the phase composition of efflorescences forming possibly in the spring time. The samples were taken in April from the same places of the Ratusz tor niche as the summer ones. The efflorescences have the form of white, very fine-grained powder accumulations.

Laboratory investigations were focused on mineralogical and geochemical analyses of the summer efflorescences using scanning electron microscopy with energy dispersive spectrometry (SEM-EDS) (FEI Company, Fremont, CA, USA), X-ray diffractometry (XRPD) (RIGAKU Corporation, Tokyo, Japan), electron microprobe analysis (EPMA) (JEOL, Tokyo, Japan), and Raman microspectroscopy (RS) (Thermo Scientific, Waltham, MA, USA). The spring efflorescences were analyzed using the XRPD method only.

The samples of summer efflorescences were studied using a FEI 200 Quanta FEG scanning electron microscope with an EDS/EDAX spectrometer. The maximum excitation voltage was 20 kV and the pressure 60 Pa (the low vacuum mode). The samples were not coated and included the efflorescences and their fragments mounted in 1 inch resin discs.

The X-ray diffractometry (XRPD) studies were performed on a whole powdered samples of the efflorescence (separation of pure pickeringite from a sample was impossible because the mineral components of the samples were extremely tiny and undistinguishable) using a Rigaku Smart Lab 90 kW diffractometer with Cu-Kα radiation. The diffractometer was equipped with a reflective graphite monochromator. The XRD patterns were recorded in the range of 3–72° 2θ with the step size of 0.02°, counting time of 2 s/step at a voltage of 45 kV, and current of 200 mA. Quartz from Jegłowa, Poland, was used as an internal standard. The unit cell parameters were refined for the monoclinic space group $P2_1/c$ in accordance with the data of the ICDD database (card no. 46-1454) and those of Quartieri et al. [1], using the least-squares method when applying the DHN-PDS program. The calculations were made on the basis of thirteen pickeringite reflections not coinciding with the reflections of other components of the efflorescence.

Quantitative chemical analyses (electron microprobe analyses (EPMA)) were carried out using a JEOL Super Probe JXA-8230 operating in the wavelength-dispersive X-ray spectroscopy (WDXS) mode under the following conditions: an accelerating voltage of 15 kV, a beam current of 1 nA, a

beam size of 7–10 μm, a peak count time of 20 s, and background time of 10 s. The EPMA operating conditions, standards, and detection limits are contained in Table 1. The Jeol ZAF procedure was used for the matrix correction of the raw data. Atomic contents of the formulae of pickeringite were calculated on the basis of 16 oxygen atoms per formula unit (apfu) with the assumed presence of 22 water molecules pfu. For the EPMA analyses, fragments of the efflorescence were mounted in 1 inch resin discs, polished using oil and coated with carbon.

Table 1. Electron microprobe analysis (EPMA) conditions for the STNR pickeringite analysis.

| Element	Signal	WDXS Crystal	Calibrant	Detection Limit [ppm] [1]
Na	$K\alpha$	TAP	albite	1780
Si	$K\alpha$	TAP	albite	1260
P	$K\alpha$	PET	fluorapatite	3150
Mn	$K\alpha$	LIF	rhodonite	4510
Fe	$K\alpha$	LIF	fayalite	2000
Sr	$L\alpha$	PET	celestine	3850
Cu	$K\alpha$	LIF	cuprite	2780
K	$K\alpha$	PET	sanidine	470
Ba	$L\alpha$	PET	barite	1350
Ca	$K\alpha$	PET	diopside	530
Zn	$K\alpha$	LIF	willemite	3000
Al	$K\alpha$	TAP	albite	1600
Pb	$M\alpha$	PET	crocoite	2900
S	$K\alpha$	PET	anhydrite	2260
Mg	$K\alpha$	TAP	diopside	1260

[1] Detection limit were determined by using JEOL software for 3σ confidence level.

The Raman spectra were recorded using a Thermo Scientific DXR Raman microscope with a 900 grooves/mm grating and a CCD detector. The Olympus 10× (NA 0.25) and 50× (NA 0.50) objectives (theoretical spot sizes 2.1 μm and 1.1 μm, respectively) were used. The sample was excited with a 532-nm laser with the maximum power of 10 mW. The laser power varied in the 3–10 mW range, selected to obtain spectra of the best quality. The spectra were recorded at an exposure time of 3 s and the number of exposures varied from 10 to 100. The spectra identification was performed using an in-house and the RRUFF Raman Minerals spectral libraries as well as some literature data [2,3,7]. The band component analysis was undertaken using the Omnic software package, which enables the type fitting function to be selected and allows specific parameters to be fixed or varied accordingly. Band fitting was carried out using a Gauss-Lorentz cross product function with the minimum number of component bands used for the fitting process.

5. Results

### 5.1. Scanning Electron Microscopy (SEM-EDS)

Pickeringite crystals found as one of the components of the white-beige summer efflorescence in the form of botryoidal aggregates occur in a complex mixture with other sulfates. The mineral paragenesis is represented mainly by alunogen $Al_2(SO_4)_3 \cdot 17H_2O$, with an admixture of gypsum $CaSO_4 \cdot 2H_2O$. Pickeringite forms aggregates of very fine and thin acicular crystals, not exceeding several hundred μm in length (Figure 3a). According to EDS analyses, they are composed of Mg, Al, S, and O with traces of Mn but without Fe, thus corresponding to the Mg-Mn joints rather than to Mg-Fe ones of halotrichites [2–4,10]. The flake crystals are composed of Al, S, and O only and represent alunogen $Al_2(SO_4)_3 \cdot 17H_2O$ (Figure 3a,b). The elemental composition of the prismatic crystals includes Ca, S, and O, so the habit and chemistry clearly identify gypsum.
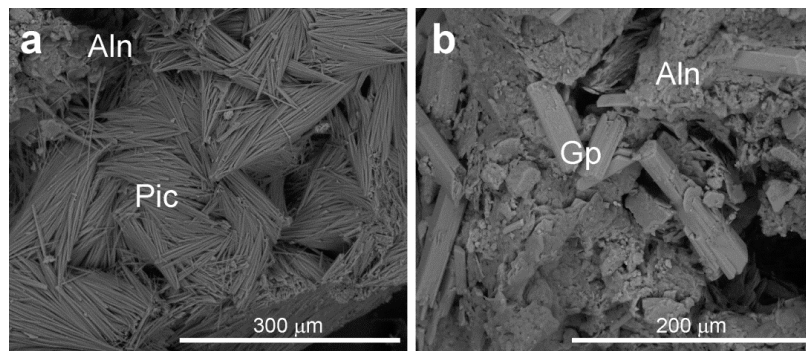
Figure 3. Back scattered electron (BSE) images of the components of the botryoidal efflorescences (**a**,**b**). Abbreviations: Aln, alunogen; Gp, gypsum; Pic, pickeringite.

5.2. X-Ray Diffractometry (XRPD)

The XRPD patterns recorded for powdered samples of the summer efflorescences reveal the presence of salt mixtures: alunogen $Al_2(SO_4)_3 \cdot 17H_2O$, pickeringite $MgSO_4 \cdot Al_2(SO_4)_3 \cdot 22H_2O$ (solid solution pickeringite-apjohnite), and traces of gypsum (Figure 4).
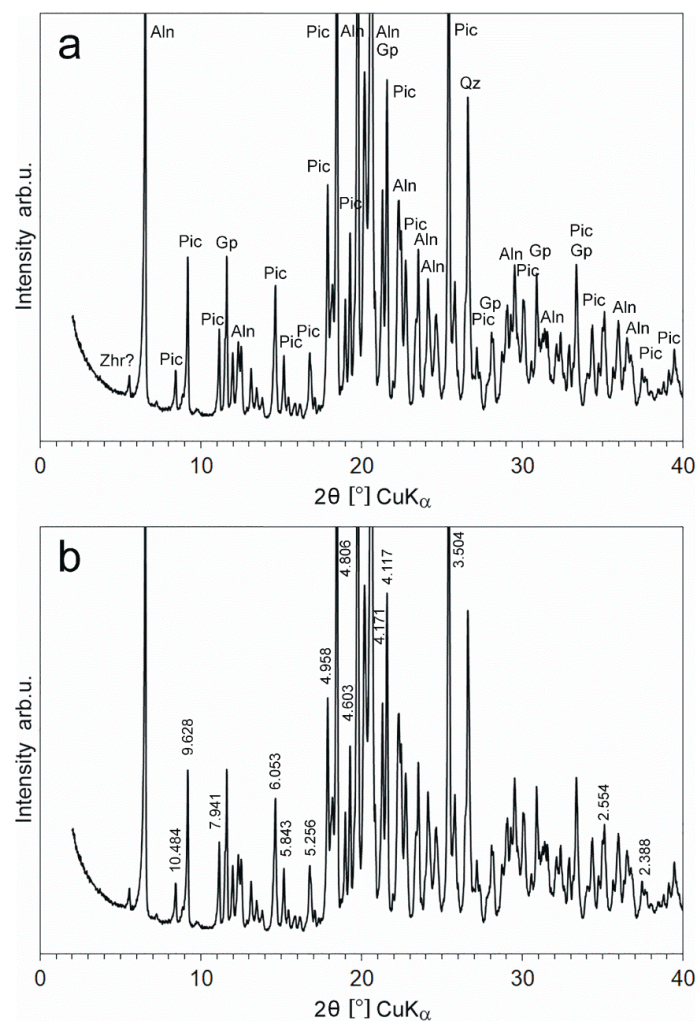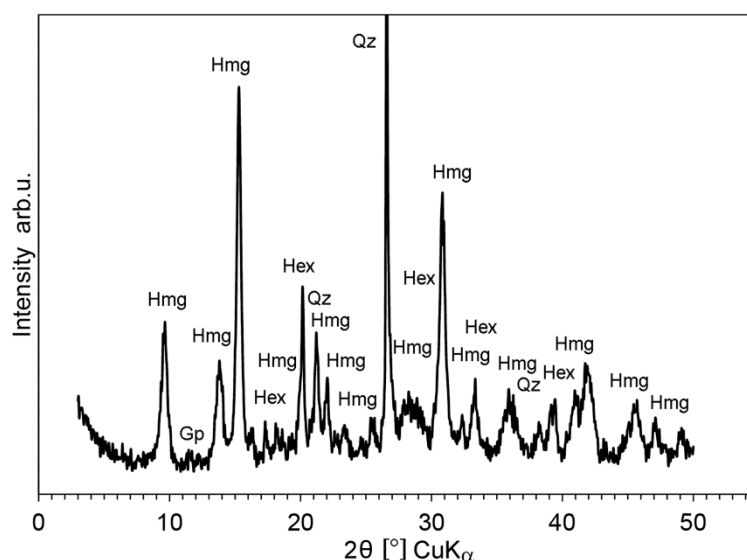

Figure 4. Characteristic X-ray patterns of the summer-formed efflorescences from the Ratusz tor (**a**) and the pickeringite reflections used for the refining unit cell parameters (**b**). Abbreviations: Aln, alunogen; Gp, gypsum; Pic, pickeringite; Qz, quartz; Zhr, zaherite.

Two rare sulfates were identified based on the following data: alunogen, the ICDD database card no. 26-1010, and pickeringite, the ICDD database card no. 46-1454 and from Quartieri et al. [1]. However, some positions of X-ray reflections and their intensities are similar to apjohnite, card no. 29-0886; gypsum was identified based on the ICDD card no. 33-311. The presence of a reflection at 15.8 Å can be assigned, according to Quartieri et al. [1] to pickeringite, although the ICDD card no. 46-1454 of this phase does not quote this reflection. Therefore, this reflection could also suggest the presence of zaherite $Al_{12}(SO_4)_5(OH)_{26} \cdot 20H_2O$ but in its dehydrated form (ICDD 29-0088). However, its identification in the efflorescences is very tentative because zaherite gives only one strong reflection 15.8 Å while three other reflections are weak and do not exceed an intensity of 8 in the relative 1–100 scale [56].

The unit cell parameters of pickeringite from STNR, refined for the monoclinic system space group $P2_1/c$, are as follows: $a = 6.1981$ (28) Å, $b = 24.2963$ (117) Å, $c = 21.2517(184)$ Å, $\beta = 100.304$ (65)°, $V = 3148.7$ Å^3.

The XRPD patterns of the spring efflorescences do not reveal the presence of pickeringite. The material consists of hydromagnesite $Mg_5[(CO_3)_4(OH)_2] \cdot 4H_2O$ with admixtures of hexahydrite $MgSO_4 \cdot 6H_2O$ and gypsum (Figure 5). These minerals were identified based on the following ICDD database cards: hydromagnesite, no. 25-513; hexahydrite, no. 24-719; and gypsum, no. 33-311. Quartz present in the samples comes from a parent rock and was identified based on the ICDD card no. 33-1161.

Figure 5. Characteristic X-ray patterns of the spring formed efflorescences from the Ratusz tor. Abbreviations: Gp, gypsum; Hex, hexahydrite; Hmg, hydromagnesite; Qz, quartz.

5.3. Chemical Analyses (EPMA)

The general formula of the halotrichite group is $XY_2(SO_4)_4 \cdot 22H_2O$, where X is divalent (mainly Co^{2+}, Fe^{2+}, Mg^{2+}, Mn^{2+}, Ni^{2+} and Zn^{2+}) and Y is trivalent (Al^{3+}, Cr^{3+} and Fe^{3+}) cations [1,5]. In this study, Fe has been calculated as FeO, so the total quantity of Fe has been assigned to the X site, indicating that the Y site is filled with Al^{3+} only (2.02 *apfu* on average) (Table 2). The X site is dominated by Mg (0.75 *apfu* on average) with an admixture of Mn (0.21 *apfu* on average). Other elements, Fe^{2+} and Cu, occur in traces (≤0.01 *apfu* on average) and Zn in minor amounts (0.02 *apfu* on average). The studied STNR pickeringite has the calculated formula $Mg_{0.75}Mn_{0.21}Zn_{0.02}Cu_{0.01}Al_{2.02}(S_{0.99 \text{ to } 1.00}O_4)_4 \cdot 22H_2O$. The presence of Na ($Na_2O$ 0.25 wt. % on average), K (K_2O 0.05 wt. % on average), Ba (BaO 0.04 wt. % on average), Sr (SrO 0.07 wt. % on average), and Ca (CaO 0.05 wt. % on average) is problematic. These elements probably come from neighboring minerals (e.g., gypsum) and/or thin clay material from the efflorescences, and they were passed over in the formula.

**Table 2.** Representative chemical compositions of the STNR pickeringite.

Analysis Number	20	31	32	35	Average	sd
wt. %						
SO_3	36.49	36.33	36.35	37.14	36.58	0.38
P_2O_5	0.03	0.11	0.03	0.00	0.04	0.05
Al_2O_3	11.64	11.87	12.22	11.65	11.85	0.27
CuO	0.00	0.06	0.11	0.13	0.08	0.06
ZnO	0.18	0.39	0.20	0.10	0.22	0.11
SrO	0.00	0.00	0.06	0.23	0.07	0.11
MnO	2.31	1.50	1.75	1.12	1.67	0.50
FeO	0.07	0.00	0.05	0.00	0.03	0.03
CaO	0.06	0.07	0.01	0.08	0.05	0.03
BaO	0.08	0.00	0.07	0.00	0.04	0.04
MgO	3.26	3.50	3.51	3.73	3.50	0.19
Na_2O	0.00	0.63	0.14	0.21	0.25	0.27
K_2O	0.02	0.05	0.06	0.07	0.05	0.02
H_2O *	45.31	45.56	45.66	45.91	45.61	0.25
Total	99.44	100.01	100.23	100.36	100.01	0.41
Apfu **						
S^{6+}	3.99	3.97	3.95	4.02	3.98	0.03
P^{5+}	0.00	0.01	0.00	0.00	0.00	0.00
Σ	3.99	3.98	3.95	4.02	3.98	0.02
Al^{3+}	2.00	2.04	2.08	1.98	2.02	0.04
ΣY	2.00	2.04	2.08	1.98	2.02	0.04
Cu^{2+}	0.00	0.01	0.01	0.01	0.01	0.01
Zn^{2+}	0.02	0.04	0.02	0.01	0.02	0.01
Mn^{2+}	0.29	0.19	0.22	0.14	0.21	0.05
Fe^{2+}	0.01	0.00	0.01	0.00	0.00	0.00
Mg^{2+}	0.71	0.76	0.76	0.80	0.75	0.03
ΣX	1.03	1.00	1.02	0.96	1.00	0.03
H_2O	22	22	22	22	22	

sd—standard deviation. * calculated from stoichiometry. ** calculated on the basis of 16 O atoms per formula unit (apfu) with the presence of 22 H_2O molecules pfu

The compositional variations of the pickeringite analyses (Table 2) are also presented in Figure 6 and confirm that the sulfate belongs to the pickeringite–apjohnite series.

5.4. Raman Microspectroscopy (RS)

The spectra in the region of 950–1000 cm^{-1} (Figure 7) display the strong band at 994 cm^{-1} assigned to the ν_1 (SO_4) symmetric stretching mode. The second, low-intensity band at 975 cm^{-1} is assigned also to the ν_1 (SO_4) mode. The bands in the region of 1000–1250 cm^{-1} are of very low intensities. Those at 1081, 1123, and 1145 cm^{-1} have been assigned to the ν_3 (SO_4) anti-symmetric stretching mode (Figure 7). The bands in the low-wave number region (Figure 8) are located at 524, 467, 425 cm^{-1} and have been assigned to the ν_2 bending mode. The ν_4 (SO_4) mode is suggested for the band at 615 cm^{-1}. Bands at 344 and 310 cm^{-1} can be attributed to the ν_g H_2O and 223 cm^{-1} to the lattice modes.
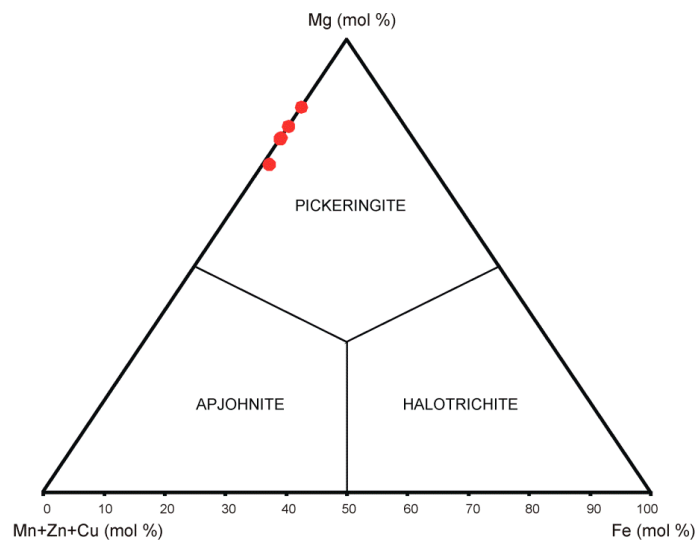
**Figure 6.** Compositional variation of the STNR pickeringite (mol. %) plotted in the Mg-Mn+Zn+Cu-Fe diagram [10].
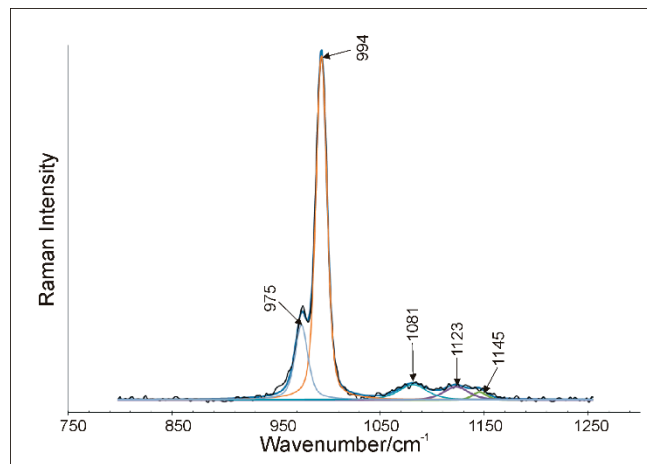
Figure 7. Raman spectra of the STNR pickeringite in the 950–1250 cm^{-1} region.
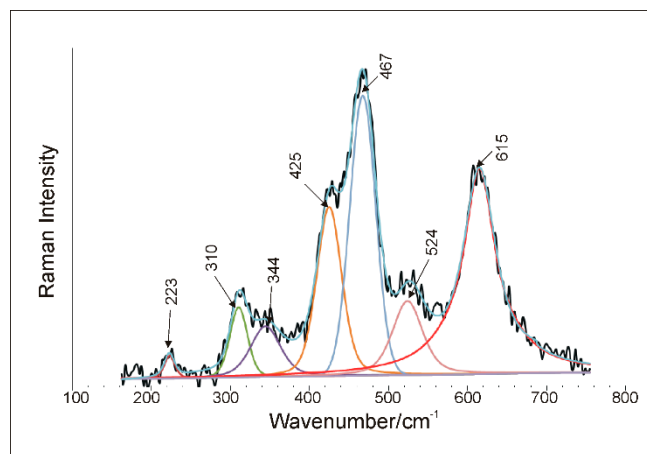
Figure 8. Raman spectra of the STNR pickeringite in the 200–700 cm^{-1} region.

The OH stretching region contains a broad band with a very low intensity between 2700 and 3500 cm^{-1} (Figure 9). Its more characteristic bands at 3012, 3275, and 3394 cm^{-1} have been assigned to the ν_3 OH stretching mode of H_2O. The identification of the Raman spectra is reported in Table 3.
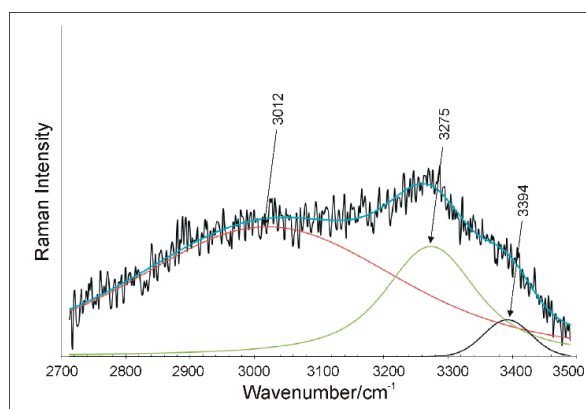
Figure 9. Raman spectra of the STNR pickeringite: stretching OH vibrations in the 2700–3500 cm^{-1} region.

**Table 3.** The Raman bands with their assignments for pickeringite and apjohnite (natural and synthetic samples).

Raman Bands (cm^{-1})						
Pickeringite	Apjohnite [1]	Apjohnite [2]	Pickeringite [2]	Apjohnite [3]	Pickeringite [4]	
This Study	Frost et al. [4]	Palmer & Frost [3]		Locke et al. [7]		Assignments [5]
3394	3490	3554	3506	3548	3449	OH stretch ν_3 (B$_g$) H_2O
		3486	3437			
3275	3394	3404	3289	3426	3279	OH stretch ν_3 (A$_g$) H_2O
3012	3490	3282		3270	3082	
	3281	3175				OH stretch ν_1 H_2O
	3281	3053				
	2925	2900				
	1658					ν_2 (B$_g$) H_2O
	1620					ν_2 (A$_g$) H_2O
1145	1113				1145	ν_3 (A$_g$) SO$_4$
1123	1148	1141	1096	1147	1114	
1081	1088			1086	1071	ν_3 (B$_g$) SO$_4$
	1070	1080	1058			
	1051			1031		
994	997	995	984	985	996	ν_1 (A$_g$) SO$_4$
	991	990	971			
975	975	975			975	
		963				
615	617	618	611	622	621	ν_4 (B$_g$) SO$_4$
			459			ν_4 (A$_u$) SO$_4$ or ν^Y (B$_g$) H_2O
524	530		445		530	ν_2 (A$_g$) SO$_4$
467	466	474	366	467	468	
425	427	460				
		423		443	424	
344	336			364	344	ν_g (A$_g$) H_2O
310	313				315	
	264		251	247		
223		204	233	214	221	lattice modes
		173	167			
		154	151			
		141				
		112				

[1] Terlano, Boltzano, Italy; composition: $Mn_{0.64}^{2+}Mg_{0.28}Zn_{0.06}Fe_{0.02}$ (after [4]). [2] synthetized; compossition: pure (after [3]). [3] Terlano, Italy; composition: $Mn_{0.64}^{2+}Mg_{0.28}Zn_{0.08}$ (after [7]). [4] San Bernardino, California; composition: $Fe_{0.22}^{2+}Mg_{0.78}$ (after [7]). [5] Band assignment follows [2,3,57,58].

6. Discussion and Concluding Remarks

6.1. Chemical Characteristics and Unit Cell Parameters of Pickeringite

Extensive isomorphism in the halotrichite group minerals along the Fe-Mg-Mn-Zn joints and the similarity of their structures have been studied by Ballirano [5]. The unit cell parameters of the STNR pickeringite with the calculated formula $Mg_{0.75}Mn_{0.21}Zn_{0.02}Cu_{0.01}Al_{2.02}(S_{0.99\ to\ 1.00}O_4)_4 \cdot 22H_2O$, determined on the basis of X-ray powder patterns, has been compared with the data of synthetic Mg-Mn joints and other available literature data on natural halotrichites enriched in Mn (Figure 10) [1,4,8,16]. The results of the unit-cell refinement are in good agreement with those from the literature and confirm a close similarity between the structures of apjohnite and pickeringite. A replacement in the pickeringite structure of Mg^{2+} ions by Mn^{2+} (Mn → Mg) with the ionic radii $r_{Mn}^{2+} = 0.83$ Å vs $r_{Mg}^{2+} = 0.72$ Å (according to Shannon, *vide* [5]) and atomic masses 54.93 vs 24.30 u, respectively, results in a nearly linear increase of the *a*, *b*, and *c* unit cell parameters and a decrease in the *β* angle [5].
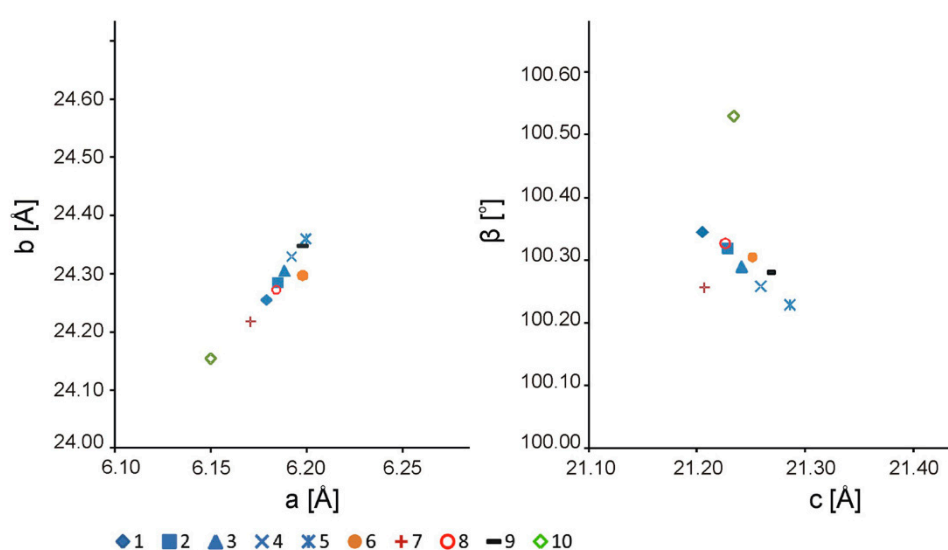
Figure 10. Unit cell parameters of the STNR pickeringite compared to literature data [1,4,5,8,16]. Explanations: 1–4, synthetic Mg-Mn joints of the following compositions: 1, $Mg_{1.00}Mn_{0.00}$; 2, $Mg_{0.75}Mn_{0.25}$; 3, $Mg_{0.50}Mn_{0.50}$; 4, $Mg_{0.25}Mn_{0.75}$; 5, $Mg_{0.00}Mn_{1.00}$ [5]; natural specimens: 6, pickeringite from the STNR [this study]; 7, pickeringite from Czerwionka (Poland) [8]; 8, pickeringite from Roccalumera (Italy) [1]; 9, apjohnite from Terlano (Italy) [4]; 10, pickeringite from Wieściszowice (Poland) [16].

The crystal structure of the pseudo-alums that crystallize in the monoclinic space group $P2_1/c$ contains four non-equivalent SO_4 tetrahedra. One of the tetrahedra is bound to the divalent cation, and the other three are involved in complex hydrogen-bond arrays involving coordinated water molecules to both cations and to the lattice water molecules [1,4,5,59] (the crystallographical structure of halotrichite can be found at http://webmineral.com/data/Halotrichite.shtml). A substantial linearity between the mean bond distance $[Me^{2+}]^{VI}$–$H_2O(O)$ and the mean ionic radius of the cation occupying the Me^{2+} position (calculated based on % of ions in the structure) has also been observed [5]. The change of the bond lengths and bounding strengths among the divalent cation, the sulfate anion, and water [60] must be reflected in the shift of Raman bands.

6.2. Spectroscopic Characteristics

The Raman spectra of alums are based on a combination of the spectra of the sulfate ions and water. The sulfate is typically a tetrahedral oxyanion with bands at 981 (ν_1), 451 (ν_2), 1104 (ν_3), and 613 (ν_4) cm^{-1} [2,3]. If the symmetry of the SO_4^{2-} group is distorted, which results in differences in S–O

the bond lengths, multiple vibration bands may exist [2,3,60]. In the structure of halotrichites, each of four crystallographically independent sulfate ions should reveal its individual Raman spectrum [2,4]. In the ν_1 SO_4 symmetric stretching region both the bands assigned to the sulfates coordinated to the divalent cation and the sulfates in the hydration sphere of aluminum should be present [2,7]. Based on relative intensities of these two band types, the higher wavenumber band (with higher intensity) is assigned to a trivalent cation (described as caused by the sulfates in the water hydration sphere of Al), the lower wavenumber band (with lower intensity) to the divalent cation (described as caused by the sulfates coordinated to the divalent cation) [2,7]. However, in most of the Raman spectra of pseudo-alums recorded at room temperature (298 K) and reported in the literature, a coincidence of the bands results in fewer bands than expected or only a slight asymmetry (a shoulder) of the band is observed [2,7]. Better separation of these bands can reveal spectra at 77 K [2]. In the case of the STNR pickeringite (whose spectra were registered at room temperature only), the band at 994 cm^{-1} assigned to ν_1 (SO_4) does not reveal any shoulder (Figure 7) that helps separate additional bands assigned to the Me^{2+} and Me^{3+} cations in the mineral structure. The position of the SO_4^{2-} band at 994 cm^{-1} corresponds to that determined by Locke et al. [7], but the Raman spectra obtained by them reveal two overlapping bands. Another band in this region has been assigned followed Ross [2,7] to water librational mode, and is also similar to that obtained by Locke et al. [7]. The Raman band positions and their assignments of pickeringite and apjohnite specimens of various origin and localization are shown in Table 3.

The number of bands observed in the ν_3 (SO_4) region should reflect the number of sulfate anions in the primitive cell, however the spectra in this region are often of not high quality because of their low intensity and/or high background [7]. The STNR pickeringite shows in this region the weak bands at 1145, 1123 and 1081 cm^{-1} (Figure 7, Table 3). In the low frequency region ν_2 three bands are observed at 524, 467 and 425 cm^{-1} (Figure 8, Table 3). The ν_4 mode is ascribed to a single band at 615 cm^{-1} showing no shoulder (Figure 8). The number of bands in respect to ν_2, ν_3 and ν_4 modes is in good agreement with the data of Locke et al. [7] (Table 3) for natural Fe-Mg pickeringite (Fe$_{0.22}$Mg$_{0.78}$). The observed number of bands in the Raman spectra at 298 K confirms the supposition that symmetry of sulfate is reduced.

The Raman spectra of the halotrichites in the OH stretching region depend on the mineral composition, however the RS is not very sensitive to the measurement of water in minerals [7]. In case of pickeringite from the STNR, its OH stretching region shows a complex band of a very low intensity. The positions of its components slightly differ from those given in the literature (Table 3).

Pickeringite is known to form continuous solid solutions not only with halotrichite but also with apjohnite. Possibilities of extensive isomorphism, and similarity of the structures result in close unit cell parameters of these minerals. However, a replacement of Mg^{2+} by Mn^{2+} (of various ionic radii and atomic masses) must somehow affect unit cell parameters and the Raman spectra [5]. As a result, even minor differences of the crystal structure change bond lengths and bounding strengths between the divalent cation, the sulfate anion and water [60]. However, based on available but scarce data regarding the halotrichites of the Mg-Mn joints [2–4,7], no clear and simple trend was observed to draw conclusions on the position of the Raman bands associated with the Mn → Mg replacement. The variation of the Raman spectrum with increasing substitution of Mn^{2+} for Mg^{2+} needs to be further explored.

6.3. Possible Origin

Pickeringite co-existing with alunogen and gypsum is a secondary mineral, found in the efflorescences of the rain-protected niche in the Ratusz (Town Hall) tor of the stone town (STNR) in Ciężkowice. Minerals of the halotrichite group usually precipitate at a low pH (2–4.5) and a high saturation of parent solutions [9,61]. These highly hydrated minerals are also characterized by a significant water solubility, so their occurrence in a moderately moist climate depends on weather conditions. Their occurrence is limited to summer periods with humidity not too high but remaining

at a sufficient level ensuring the crystallization of the mineral which theoretically contains ~46% H_2O. Such conditions are met, e.g., in a niche which shelters the minerals from dissolving. They occur in the Ratusz (Town Hall) tor, located slightly above the floodplain of the Biała River and permanently damp in its lower parts. The tor position provides enough moisture for the crystallization of highly hydrated salts such as pickeringite and coexisting alunogen during the summer period.

However, despite the seasonal or temporal changes of the prevailing atmospheric conditions (temperature, humidity), salt efflorescences still form there, but their mineral composition also changes. In the early spring (April) at about 12 °C, hydromagnesite $Mg_5[(CO_3)_4(OH)_2]\cdot4H_2O$ is the predominant component, while hexahydrite $MgSO_4\cdot6H_2O$ and gypsum are admixtures. These efflorescences appear in the same place as pickeringite in the summer period, and occur in the vicinity of and along the fractures, which may point to a significant role of water solutions migrating through the rock mass.

Generally, the environment where hydromagnesite currently precipitates is characterized by high pH and high Mg/Ca ratios [62–64]. It is by far the most common, naturally occurring mineral phase belonging to the group of hydrated Mg-carbonates (i.e., containing hydroxyl groups) of the MgO-CO_2-H_2O system [63,64]. This may be explained by the high hydration energy of the Mg^{2+} cation that prevents the formation of anhydrous $MgCO_3$ phases. Globally the hydromagnesite occurrences are linked to weathering of magnesium-rich rocks, lacustrine, or marine precipitates and alkaline wetlands, but also bricks and mortars and even weathered meteorites [62,63].

The presence of hydromagnesite that crystallizes under a clearly alkaline pH, while pickeringite precipitates in acid environments, indicates a strong variability of the environmental parameters depending on the seasonal weather conditions. At times when highly acid conditions prevail, pickeringite and alunogen (the latter also needs low pH) form, but if acid sulfate-bearing solutions are diluted by rain falls, snow, fog etc., these two phases become unstable and dissolve, whereas the increasing pH values stabilize other phases, e.g., hydromagnesite.

The presence of sulfate ions and low pH values in the range of 2–4.5 favored eventually the crystallization of pickeringite [9–11,16]. The generation of the sulfate ions was ensured by the oxidation of pyrite, which is corroborated by frequent goethite pseudomorphs after iron sulfide in the surface rock layers of the Ratusz tor (Figure 11). The crystallization of various sulfate salts within this particular tor is thus controlled by a set of necessary conditions of a climatic (e.g., season, temperature, humidity), physicochemical (e.g., pH, concentration), mineralogical (the presence of pyrite), and site-related (location and protection of efflorescences) nature.
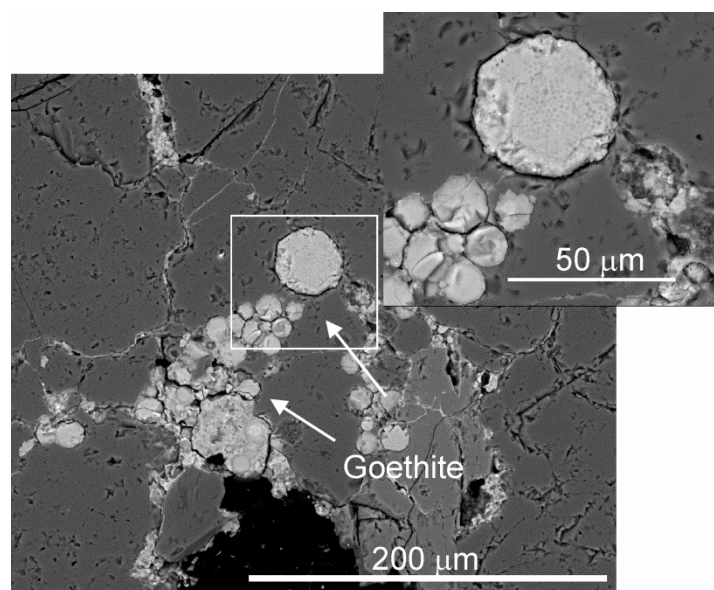
Figure 11. Back scattered electron (BSE) images of the characteristic goethite pseudomorphs after pyrite from the weathered part of the Ratusz tor sandstone.

Thus, if the rocks of other tors do not contain enough pyrite, the whole chain of the events mentioned cannot even start and pickeringite never precipitates. The same will happen if the rock is not damp enough, which depends on the tor position across the river valley and an elevation of the water table [38] etc.

In turn, the Ciężkowice sandstones are carbonate-free or very low in carbonates, thus there are no buffer minerals that can reduce the acidity of the rock environment. For this reason, a lower pH of pore solutions within these rocks is maintained for a longer time. Under such conditions a range of aluminosilicate minerals decompose and liberate cations of aluminium, magnesium, and manganese forming later the Al-rich salts, i.e., pickeringite and alunogen, of the efflorescences. In case of the Ratusz tor sandstone, such minerals include the mica group, mainly biotite, and feldspars (plagioclases). Kaolinite, illite, glauconite, as well a small amount of the interstratified illite-smectite group minerals identified in the matrix of the Ciężkowice sandstones, can also provide these cations [38,51,52].

Another source of the pickeringite- and alunogen-forming ions may be represented by waters circulating in the rocks from different levels of the Carpathian flysch. This problem has been discussed in detail by Alexandrowicz and Marszałek [38]. The Ciężkowice Foothills is the region characterized by sulfurous spring waters [65] containing H_2S, whose presence is explained as its being a product of pyrite (FeS_2) decomposition during weathering [66]. This mineral is rather a common but minor component of the Carpathian flysch strata [45]. However, as the sandstone complexes with a high permeability prevail in the geological structure of the Ciężkowice Foothills, they form conduits of possible mixing of waters of various provenience and from various circulation horizons. So, the origin of sulfur of the efflorescences could be traced back either to a direct transformation of pyrite into secondary minerals or to waters enriched in hydrogen sulfide. In both cases it means that pyrite contained in the sandstones of the Carpathian flysch, including the Ciężkowice sandstones, is the initial source of sulfur.

The presence of sulfate secondary minerals is often attributed to a direct impact of the polluted atmosphere and the air precipitations contaminating groundwater (e.g., [67–70]). Although the reports on the quality of the environment near the Ciężkowice area have not identified hazards caused by excessive sulfur, the possible contribution of the air pollution cannot be ruled out, mainly due to its long-term impact [38]. Nevertheless, in the case of the Ratusz tor, the role of this source in crystallization of pickeringite should be considered as marginal.

Isotopic analyses could put the light on the problem of identifying sources of sulfur taking part in formation of pickeringite and other sulfate-bearing efflorescences from the Stone Town Nature Reserve. A respective complementary research program is planned as a follow-up of the investigations presented here.

References

1.   Quartieri, S.; Triscari, M.; Viani, A. Crystal structure of the hydrated sulphate pickeringite ($MgAl_2(SO_4)_4$ $22H_2O$): X-ray powder diffraction study. *Eur. J. Miner.* **2000**, *12*, 1131–1138. [CrossRef]

2.   Frost, R.L.; Kloprogge, J.T.; Williams, P.A.; Leverett, P. Raman microscopy of some natural pseudo-alums: Halotrichite, apjohnite and wupatkiite, at 298 and 77 K. *J. Raman Spectrosc.* **2000**, *31*, 1083–1087. [CrossRef]

3.   Palmer, S.; Frost, R.L. Synthesis and spectroscopic characterization of apjohnite and pickingerite. *Polyhedron* **2006**, *25*, 3379–3386. [CrossRef]

4.   Menchetti, S.; Sabelli, C. The halotrichite group: The crystal structure of apjohnite. *Mineral. Mag.* **1976**, *40*, 599–608. [CrossRef]

5.   Ballirano, P. Crystal chemistry of the halotrichite group $XAl_2(SO_4)_4 \cdot 22H_2O$: The X = Fe-Mg-Mn-Zn compositional tetrahedron. *Eur. J. Miner.* **2006**, *18*, 463–469. [CrossRef]

6.   Hammarstrom, J.M.; Smith, K.S. Geochemical and mineralogical characterization of solids and their effects on waters in metal-mining environments. In *Progress on Geoenvironmental Models for Selected Mineral Deposit Types*; Seal, R.R., II, Foley, N.K., Eds.; US Geological Survey Open-File Report 02-195; US Geological Survey: Reston, VA, USA, 2002; pp. 9–54.

7.   Locke, A.J.; Martens, W.N.; Frost, R.L. Natural halotrichites-an EDX and Raman spectroscopic study. *J. Raman Spectrosc.* **2007**, *38*, 1429–1435. [CrossRef]

8.   Kruszewski, Ł. Supergene sulphate minerals from the burning coal mining dumps in the Upper Silesian Coal Basin, South Poland. *Int. J. Coal Geol.* **2013**, *105*, 91–109. [CrossRef]

9.   Parnell, R.A., Jr. Weathering processes and pickeringite formation in a sulfidic schist: A consideration in acid precipitation neutralization studies. *Environ. Geol.* **1983**, *4*, 209–215. [CrossRef]

10.   Hammarstrom, J.M.; Seal, R.R., II; Meier, A.L.; Kornfeld, J.M. Secondary sulfate minerals associated with acid drainage in the eastern, US: Recycling of metals and acidity in surficial environments. *Chemic. Geol.* **2005**, *215*, 407–431. [CrossRef]

11.   Farkas, I.M.; Weiszburg, T.G.; Pekker, P.; Kuzmann, E. A half-century of environmental mineral formation on a pyrite-bearing waste dump in the Mátra mountains, Hungary. *Can. Mineral.* **2009**, *47*, 509–524. [CrossRef]

12.   Mladenova, V.; Dimitrova, D.; Schmitt, R.F. Efflorescent minerals formed during intensive weathering of phyllites, Chiprovtsi ore district, Northwestern Bulgaria. In Proceedings of the Annual Conference of Bulgarian Geological Society (Geosciences-2007), Sofia, Bulgaria, 13–14 December 2007; pp. 63–64.

13.   Gomes, P.; Valente1, T.; Grande, J.A.; Cordeiro, M. Occurrence of sulphate efflorescences in São Domingos mine. *Comun. Geológicas* **2017**, *104*, 83–89.

14.   Martin, R.; Rodgers, K.A.; Browne, P.R.L. The nature and significance of sulphate-rich, aluminous efflorescences from the Te Kopia geothermal field, Taupo Volcanic Zone, New Zealand. *Mineral. Mag.* **1999**, *63*, 413–419. [CrossRef]

15.   Parafiniuk, J. Fibroferrite, slavikite and pickeringite from the oxidation zone of pyrite-bearing schists in Wieściszowice (Lower Silesia). *Mineral. Pol.* **1991**, *22*, 3–15.

16.   Parafiniuk, J. Sulphate minerals and their origin in the weathering zone of the pyrite-bearing schist at Wieściszowice (Rudawy Janowickie Mts., Western Sudetes, Poland). *Acta Geol. Pol.* **1996**, *46*, 353–414.

17. Naglik, B.; Natkaniec-Nowak, L. Pickeringite from the Pieprzowe Mts. (the Holy Cross Mts., Central Poland). *Geol. Geoph. Environ.* **2015**, *41*, 114–115. [CrossRef]

18. Jambor, J.L.; Nordstrom, D.K.; Alpers, C.N. Metal-sulfate salts from sulfide mineral oxidation. In *Sulfate Minerals Crystalography, Geochemistry and Environmental Significance*; Alpers, C.N., Jambor, J.L., Nordstrom, D.K., Eds.; Reviews in Mineralogy & Geochemistry; Mineralogical Society of America, Geochemical Society: Washington, DC, USA, 2000; Volume 40, pp. 303–350. [CrossRef]

19. Blass, G.; Strehler, H. Mineralbildungen in einer durch Selbstentzündung brennenden Bergehalde des Aachener Steinkohlenreviers. *Miner. Welt* **1993**, *4*, 35–42. (In German)

20. Bouška, V.; Dvořák, Z. *Minerals of the North Bohemian Lignite Basins*; Nakl.: Dick, Praha, 1997; pp. 1–159. (In Czech)

21. Jírasek, J. *Thermal Changes of the Rocks in the Dump Pile of the Kateřina Colliery in Radvanice (Eastern Bohemia)*; VSB-Technical University of Ostrava, Institute of Geological Engineering: Ostrava, Czechia, 2001; Volume 541, p. 69.

22. Szakáll, S.; Kristály, F. Ammonium sulphates from burning coal dumps at Komló and Pécs-Vasas, Mecsek Mts., South Hungary. *Mineral. Spec. Papers* **2008**, *32*, 155.

23. Brant, R.A.; Foster, W.R. Magnesian Halotrichite from Vinton County, Ohio. *Ohio J. Sci.* **1959**, *59*, 187–192.

24. Vorma, A. Sulfide-bearing mica gneiss containing pickeringite. *Bull. Comm. Geol. Finlinde* **1966**, *38*, 51–53.

25. Suchý, V.; Sýkorová, I.; Zachariáš, J.; Filip, J.; Machovič, V.; Lapčák, L. Hypogene Features in Sandstones: An Example from Carboniferous Basins of Central and Western Bohemia, Czech Republic. In *Hypogene Karst Regions and Caves of the World*; Klimchouk, A.W., Palmer, A., De Waele, J., Auler, A.S., Audra, P., Eds.; Springer International Publishing AG: New York, NY, USA, 2017; pp. 313–328. [CrossRef]

26. Lazaridis, G.; Melfos, V.; Papadopoulou, L. The first cave occurrence of orpiment (As_2S_3) from the sulfuric acid caves of Aghia Paraskevi (Kassandra Peninsula, N. Greece). *Int. J. Speleol.* **2011**, *40*, 133–139. [CrossRef]

27. Sulovsky, P.; Gregerova, M.; Pospisil, P. Mineralogical Study of Stone Decay in Charles Bridge, Prague. In Proceedings of the 8th International Congress on the Deterioration and Conservation of Stone, Berlin, Germany, 30 September–4 October 1996; Riederer, J., Ed.; Möller Druck und Verlag: Berlin, Germany, 1996; pp. 29–36.

28. Küng, A.; Zehnder, K. Pickeringite: A deleterious salt on buildings. *Stud. Conserv.* **2017**, *62*, 304–308. [CrossRef]

29. Wieser, T. Siarczanowe produkty wietrzenia na złożu żelaza Gór Świętokrzyskich. *Ann. Soc. Geol. Pol.* **1949**, *19*, 445–477. (In Polish)

30. Kubisz, J. Studies of supergene sulphate minerals occurring in Poland. *Prace Geol.* **1964**, *26*, 1–76. (In Polish)

31. Biłoniżka, P.M. O pochodzeniu mioceńskich soli potasowo-magnezowych Przedkarpacia. *Prz. Geol.* **1996**, *44*, 1029–1031. (In Polish)

32. Gajdówna, E. *Gips i Towarzyszące mu Minerały w Dobrzyniu Nad Wisłą*; Muzeum Ziemi: Warszawa, Poland, 1952; p. 6. (In Polish)

33. Mazur, L. Rentgenograficzno-chemiczne badania siarczanowych produktów wietrzenia pirytu występującego w Dobrzyniu nad Wisłą. *Stud. Soc. Sci. Tor.* **1962**, *IV*, 2. (In Polish)

34. Parafiniuk, J. Sulphate weathering minerals from the mica schist quarry in Krobica (West Sudeten, SW Poland). *Prz. Geol.* **1994**, *7*, 536–538. (In Polish)

35. Ciesielczuk, J.; Kruszewski, Ł.; Fabiańska, M.J.; Misz-Kennan, M.; Kowalski, A.; Mysza, B. Efflorescences and gas composition emitted from the burning coal-waste dump in Słupiec, Lower Silesian Coal Basin, Poland. In Proceedings of the International Symposium CEMC 2014, Skalský Dvůr, Czech Republic, 23–26 April 2014; pp. 26–27.

36. Naglik, B.; Heflik, W.; Natkaniec-Nowak, L. Charakterystyka mineralogiczno-petrograficzna utworów klastycznych Gór Pieprzowych (Wyżyna Sandomierska) i produktów ich wietrzenia. *Prz. Geol.* **2016**, *64*, 338–343. (In Polish)

37. Naglik, B.; Natkaniec-Nowak, L.; Heflik, W. Mineral assemblages as a record of the evolutionary history of the Pepper Mts. Shale Formation (the Holy Cross Mts.). *Geol. Geoph. Envir.* **2016**, *42*, 161–173. [CrossRef]

38. Alexandrowicz, Z.; Marszałek, M. Efflorescences on weathered sandstone tors in the Stone Town Nature Reserve in Cięžkowice the Outer Carpathians, Poland-their geochemical and geomorphological controls. *Envir. Sci. Poll. Res.* **2019**, *26*, 37254–37274. [CrossRef]

39. Alexandrowicz, Z. Sandstone rocky forms in Polish Carpathians attractive for education and tourism. *Prz. Geol.* **2008**, *56*, 680–687.

40. Alexandrowicz, Z. Sandstone tors of the Western Flysch Carpathians. *Pr. Geol. Kom. Nauk Geol. PAN* **1978**, *113*, 87. (In Polish)

41. Alexandrowicz, Z. Inanimate nature in the Czarnorzecki Landscape Park. *Ochr. Przyr.* **1987**, *45*, 263–293. (In Polish)

42. Alexandrowicz, Z. Rezerwaty i pomniki przyrody nieożywionej województwa krośnieńskiego. In *System Ochrony Przyrody i Krajobrazu Województwa Krośnieńskiego*; Michalik, S., Ed.; Studia Naturae B: Kraków, Poland, 1987; Volume 32, pp. 23–72. (In Polish)

43. Alexandrowicz, Z. Sandstone rocks in the vicinity of Ciężkowice on the Biała River. *Ochr. Przyr.* **1970**, *35*, 281–335. (In Polish)

44. Cieszkowski, M.; Koszarski, A.; Leszczyński, S.; Michalik, M.; Radomski, A.; Szulc, J. *Detailed Geological Map of Poland 1:50 000 Sheet Ciężkowice*; Państwowy Instytut Geologiczny: Warszawa, Poland, 1991. (In Polish)

45. Leszczyński, S. Ciężkowice Sandstones of the Silesian Unit in the Polish Carpathians: A study of coarse-clastic sedimentation in the deep-water. *Ann. Soc. Geol. Pol.* **1981**, *51*, 435–502. (In Polish)

46. Koszarski, L. Observation on the Sedimentation of the Ciężkowice sandstone near Ciężkowice (Carpathian Flysch). *Bull. Acad. Pol. Sci.* **1956**, *3*, 393–398.

47. Leszczyński, S. Characteristics and origin of flxoturbidites from the Carpathian flysch (Cretaceous–Palaeogene). South Poland. *Ann. Soc. Geol. Pol.* **1989**, *59*, 351–390.

48. Jurkiewicz, H. Foraminifers in the sub-Menilitic Paleogene of the Polish Middle Carpathians. *Inst. Geol. Biul.* **1967**, *210*, 5–128. (In Polish)

49. Pettijohn, F.J.; Potter, P.E.; Siever, R. *Sand and Sandstone*; Springer: New York, NY, USA, 1972.

50. Leszczyński, S.; Dziadzio, P.S.; Nemec, W. Some current sedimentological controversies in the Polish Carpathian flysch. In Proceedings of the Guidebook for Field Trips Accompanying 31st IAS Meeting of Sedimentology Held in Kraków, Kraków, Poland, 22–25 June 2015; Haczewski, G., Ed.; Polish Geological Society: Kraków, Poland, 2015; pp. 247–287.

51. Bromowicz, J.; Górniak, K.; Przystaś, G.; Rembiś, M. Wyniki badań petrograficznych typowych litofacji zbiornikowych fliszu karpackiego. In *Charakterystyka Parametrów Petrofizycznych Fliszowych Serii Ropogazonośnych Karpat Polskich*; Kuśmierek, W., Ed.; Polish Journal of Mineral Resources: Kraków, Poland, 2001; Volume 4, pp. 31–75. (In Polish)

52. Alexandrowicz, Z.; Marszałek, M.; Rzepa, G. Distribution of secondary minerals in crusts developed on sandstone exposures. *Earth Surf. Process. Landf.* **2014**, *39*, 320–335. [CrossRef]

53. Alexandrowicz, Z.; Marszałek, M.; Rzepa, G. The role of weathering crust in the Evolution of surfaces on the Carpathian sandstone tors. *Chrońmy Przyr. Ojczystą* **2012**, *68*, 163–174, (In Polish with English Abstract).

54. Alexandrowicz, Z.; Pawlikowski, M. Mineral crust of the surface weathering zone of sandstone tors in the Polish Carpathians. *Mineral. Pol.* **1982**, *13*, 41–59.

55. Wilczyńska-Michalik, W. *Influence of Atmospheric Pollution on the Weathering of Stones Monuments in Cracow and Rock Outcrops in Cracow, Cracow-Częstochowa Upland and the Carpathians*; Prace Monograficzne 377 Akademia Pedagogiczna: Kraków, Poland, 2004.

56. Ruotsala, A.P.; Babcock, L.L. Zaherite, a new hydrated aluminum sulfate. *Am. Mineral.* **1977**, *62*, 1125–1128.

57. Ross, S.D. Sulphates and other oxy-anions of Group VI. In V.C. In *The Infrared Spectra of Minerals*; Farmer, V.C., Ed.; The Mineralogical Society: London, UK, 1974; pp. 423–444.

58. Griffith, W.P. Advances in Raman and infrared spectroscopy of minerals. In *Spectroscopy of Inorganic-Based Materials*; Clark, R.J.H., Hester, R.E., Eds.; John Wiley & Sons: Chichester, UK, 1987; pp. 119–186.

59. Hawthorn, F.C.; Krivovichev, S.V.; Burns, P.C. The crystal chemistry of sulfate minerals. In *Sulfate Minerals-Crystallography, Geochemistry, and Environmental Significance*; Reviews in Mineralogy and Geochemistry 40; Alpers, C.N., Jambor, J.L., Nordstrom, D.K., Eds.; Mineralogical Society of America: Washington, DC, USA, 2000; pp. 1–112.

60. Palmer, S.; Frost, R.L. Molecular structure of Mg–Al, Mn–Al and Zn–Al halotrichites-type double sulfates—An infrared spectroscopic study. *Spectrochim. Acta Part A* **2011**, *78*, 1633–1639. [CrossRef]

61. Alpers, C.N.; Blowes, D.W.; Nordstrom, D.K.; Jambor, J.L. Secondary minerals and acid mine-water chemistry. In *Short Course Handbook on Environmental Geochemistry of Sulphide Mine Wastes*; Jambor, J., Blowes, D., Eds.; Mineralogical Association of Canada: Waterloo, ON, Canada, 1994; pp. 247–270.

62. Frost, R.L. Raman spectroscopic study of the magnesium carbonate mineral hydromagnesite ($Mg_5(CO_3)_4(OH)_2 \cdot 4H_2O$). *J. Raman Spectrosc.* **2011**, *42*, 1690–1694. [CrossRef]

63. Hopkinson, L.; Kristova, P.; Rutt, K.; Cressey, G. Phase transitions in the system $MgO–CO_2–H_2O$ during CO_2 degassing of Mg-bearing solutions. *Geochim. Cosmochim. Acta* **2012**, *76*, 1–13. [CrossRef]

64. Gautier, Q.; Bénézeth, P.; Mavromatis, V.; Schott, J. Hydromagnesite solubility product and growth kinetics in aqueous solution from 25 to 75 °C. *Geochim. Cosmochim. Acta* **2014**, *138*, 1–20. [CrossRef]

65. Rajchel, J.; Marszałek, M.; Rajchel, L. Deposits of sulphurous spring waters from the Carpathians and the Carpathian Foredeep (southern Poland). *Prz. Geol.* **2000**, *48*, 1174–1180. (In Polish)

66. Rajchel, L.; Zuber, A.; Duliński, L.; Rajchel, J. Izotope and chemical composition and water ages of sulphide springs in the Polish Carpathians. In *Współczesne Problem Hydrogeologii*; Sadurski, A., Krawiec, A., Eds.; UMK Toruń: Toruń, Poland, 2005; Volume 12, pp. 583–588. (In Polish)

67. Přikryl, R.; Melounová, L.; Vařilová, Z.; Weishauptová, Z. Spatial relationships of salt distribution and related physical changes of underlying rocks on naturally weathered sandstone exposures (Bohemian Switzerland National Park, Czech Republic). *Environ. Geol.* **2007**, *52*, 409–420. [CrossRef]

68. Přikryl, R.; Svobodová, J.; Žák, K.; Hradil, D. Anthropogenic origin of salt crusts on sandstone sculptures of Prague's Charles Bridge (Czech Republic): Evidence of mineralogy and stable isotope geochemistry. *Eur. J. Miner.* **2004**, *16*, 609–618. [CrossRef]

69. Schweigstillová, J.; Přikryl, R.; Novotná, M. Isotopic composition of salt efflorescence from the sandstone castellated rocks of the Bohemian Cretaceous Basin (Czech Republic). *Environ. Geol.* **2009**, *58*, 217–225. [CrossRef]

70. Navrátil, T.; Vařilová, Z.; Rohovec, J. Mobilization of aluminum by the acid percolates within unsaturated zone of sandstones. *Environ. Monit. Assess.* **2013**, *185*, 7115–7131. [CrossRef]